Quantum emitter interacting with graphene coating in the strong-coupling regime

Mehmet Günay,[1,*] Vasilios Karanikolas,[2] Ramazan Sahin,[3] Rasim Volga Ovali,[4] Alpan Bek,[5,†] and Mehmet Emre Tasgin[2,†]

[1]*Department of Nanoscience and Nanotechnology, Faculty of Arts and Science, Mehmet Akif Ersoy University, 15030 Burdur, Turkey*
[2]*Institute of Nuclear Sciences, Hacettepe University, 06800 Ankara, Turkey*
[3]*Faculty of Science, Department of Physics, Akdeniz University, 07058 Antalya, Turkey*
[4]*Department of Materials Science and Nanotechnology Engineering, Recep Tayyip Erdogan University, 53100 Rize, Turkey*
[5]*Department of Physics, Middle East Technical University, 06800 Ankara, Turkey*

(Received 15 January 2020; revised manuscript received 13 February 2020; accepted 20 March 2020; published 14 April 2020)

We demonstrate the strong coupling of a quantum dot and a graphene spherical shell coating it. Our simulations are based on solutions of three-dimensional Maxwell equations, using a boundary element method approach. Interaction between the nanostructures produces sharp hybrid modes, even when the two are off-resonant. The coupling of the light to these "very sharp" plexcitonic resonances is an order of magnitude larger than its coupling to a quantum dot, and they are voltage tunable (continuously) in an 80-meV interval. Hence, our results are very attractive for sensing applications and graphene display technologies with sharper colors. Moreover, on a simple theoretical model, we explain why such sharp highly tunable hybrid resonances emerge.

DOI: 10.1103/PhysRevB.101.165412

I. INTRODUCTION

Graphene is a material with superior optical, electronic, and mechanical properties [1–5], and it can be used for replacing noble metals (mainly Au and Ag) for applications operating at near- to far-infrared (IR) wavelengths [6]. Graphene possesses an advantage over noble metals due to having smaller material losses [7] and tunability of its optical properties [8]. Thus, it allows to design of multipurpose applications [9–11].

In recent years, graphene has also been recognized as a promising active material in the realization of supercapacitors. Studies have shown that having large surface area is essential for such applications [12,13]. In that respect, a spherical geometry (graphene nanoball) was considered to increase the surface area. Then it was shown that a graphene mesoporous structure with an average pore diameter of 4.27 nm can be fabricated via chemical vapor deposition technique [14]. Additionally, self-crystallized graphene and graphite nanoballs have been recently demonstrated via Ni vapor-assisted growth [15]. Utilization of such growth techniques or in-liquid synthesis methods [16] can be employed to construct nanoparticle-graphene composite structures, which operate in a strong-coupling regime. In many of studies on such nanoscale composites, the focus of attention was mainly on electrical properties. It is also intriguing to study the optical applications [17,18] of the graphene spherical shell structures in terms of their plasmonic responses [19,20].

Graphene plasmons (GPs) can trap the incident light into small volumes [21,22], called hot spots. The resonance values of the GPs can be tuned continuously by applying a voltage or by electrostatic doping [23]. This tuning provides incredible potential in a vast number of applications, such as sensing [24], switching [8], and metamaterials [25]. Placing a quantum emitter (QE), such as a quantum dot (QD), in close proximity to a graphene nanostructure can yield strong interaction [21] and modulations in optical properties. Usually, the interactions between QE placed in a nanostructured environment are described by investigating the QE's lifetime and calculating the Purcell factor [21]. For such simulations, the QE-nanostructure interaction is described in terms of non-Hermitian of quantum electrodynamics, where the QE is assumed as a point dipole source. In that respect, the interaction between the QE and an infinite graphene layer has been investigated experimentally by measuring the relaxation rate related to the distance between them [26] or the chemical potential value of the graphene layer [27]. The QEs used are erbium ions with a transition energy close to the telecommunication wavelength, where the graphene nanostructures can have a plasmonic response for specific chemical potential values. Moreover, there are variety of molecules and quantum emitters also operating at infrared wavelengths [28,29].

In this paper, we demonstrate the strong coupling between a 5-nm-radius quantum dot and a graphene spherical shell, of the same size, coating the quantum dot as shown in Fig. 1(a). We show that, in this way, the strong coupling between the quantum dot and the graphene shell can be achieved even in a single quantum emitter level. A splitting of about 80 meV between the two hybrid modes could be obtained due to the strong coupling, interestingly, even when the spectrum of the quantum dot does not overlap with the graphene shell. In

*gunaymehmt@gmail.com
†These authors contributed equally to this work.

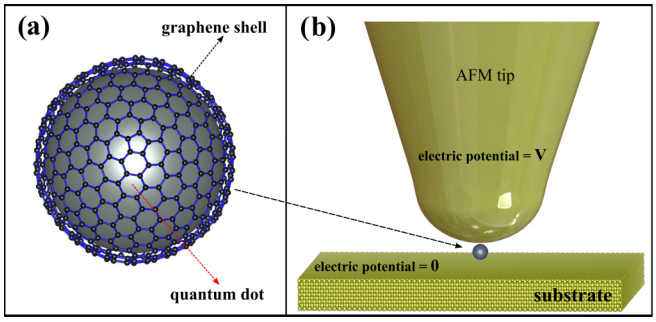

FIG. 1. (a) The hybrid structure, a QD coated with a graphene spherical shell. (b) In the proposed experimental setup, the hybrid structure is placed between the substrate and the atomic force microscopy tip with zero and finite electrical potential respectively to tailor the Fermi energy level of graphene by the applied bias voltage [30].

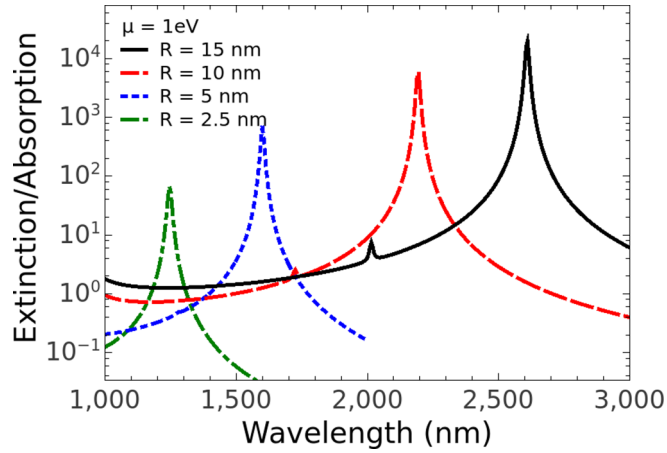

FIG. 2. Absorption spectrum of the graphene spherical shell, varying the excitation wavelength. We keep fixed the value of the chemical potential, $\mu = 1$ eV, of the graphene spherical shell for different values of its radius, $R = 2.5$, 5, 10, and 15 nm.

the off-resonant case, one of the (tunable) hybrid modes is very narrow compared to the linewidth of the bare graphene (around three times). The spectral positions of the these hybrid modes can be controlled via tuning the chemical potential of the graphene shell, which can be done by tailoring the Fermi energy level of graphene by the applied bias voltage [30] as shown in Fig. 1(b). We remark that the spectral position of a QD (in general a QE) is also tunable via the applied voltage. The coupling of light to a QD, however, is an order of magnitude lower compared to a graphene shell–QD hybrid structure, which also provides a more intense hot spot. Having such tunable hybrid modes with sharper linewidths is of importance for enhanced figure of merit (FOM) sensing and, for instance, graphene display technologies [31] with sharper color tunings. Beyond demonstrating these effects via solutions of the three-dimensional (3D) Maxwell equations obtained from the boundary element method approach (taking the retardation effects into account), we also show that the same effects are already predicted by a simple analytical model. We explain the physics, i.e., why such a sharp hybrid mode appears, simply on the analytical model.

The paper is organized as follows. We first present the solutions of the 3D Maxwell equations obtained from the boundary element method approach, specifically, the absorption spectrum of the graphene spherical shell, the semiconducting sphere individually, and the combination of a QE with a graphene spherical shell (the full case), respectively, in Sec. II. Next we describe the theoretical model and derive an effective Hamiltonian for a two-level system (QE) coupled to graphene plasmons in Sec. III, where we derive the equations of motion for suggested structure and obtain *a single equation* for the steady-state plasmon amplitude. A summary appears in Sec. IV.

II. ELECTROMAGNETIC SIMULATIONS OF THE ABSORPTION OF A GRAPHENE COATED SEMICONDUCTING SPHERE

When the absorption peak of the QE matches the graphene plasmon resonance, we observe a splitting in the absorption band due to the interaction between the exciton-polariton mode, of the semiconducting sphere, with the localized surface plasmon mode, supported by the graphene spherical shell. To prove this, we perform electromagnetic simulations by using the MNPBEM package [32], through solving the Maxwell equations in three dimensions. This splitting is connected to the energy exchange between the two modes. Due to the large splitting the system enters the strong-coupling regime, where a splitting of 80 meV between the hybrid modes is observed [33]. These types of collective modes have been also named as plexcitons [34]. We stress out that the QE coated with graphene spherical shell has been experimentally demonstrated [35]. In this section, we start with presenting the mathematical framework and the expressions that give the dielectric permittivity of the graphene spherical shell and of the semiconducting QE. Next we present results regarding the absorption spectrum of the graphene spherical shell, the QE, and the full case of QE with a graphene spherical shell coating.

The optical response of graphene is given by its in-plane surface conductivity, σ, in the random-phase approximation [36,37]. This quantity is mainly determined by electron-hole pair excitations, which can be divided into intraband and interband transitions $\sigma = \sigma_{\text{intra}} + \sigma_{\text{inter}}$. It depends on the chemical potential (μ), the temperature (T), and the scattering energy (E_S) values [38].

The intraband term σ_{intra} describes a Drude modes response, corrected for scattering by impurities through a term containing τ, the relaxation time. The relaxation time, τ, causes the plasmons to acquire a finite lifetime and is influenced by several factors, such as collisions with impurities, coupling to optical phonon, and finite-size effects. In this paper, we assume that $T = 300$ K and $\tau = 1$ ps. In addition, we vary the value of chemical potential [9], μ, for active tuning of graphene plasmons.

In Figs. 2 and 3, we present the extinction spectrum of the graphene spherical shell by a plane-wave illumination. In both figures, we observe a peak in the extinction spectrum. This peak value is due to the excitation of localized surface plasmon (LSP) mode supported by the graphene spherical

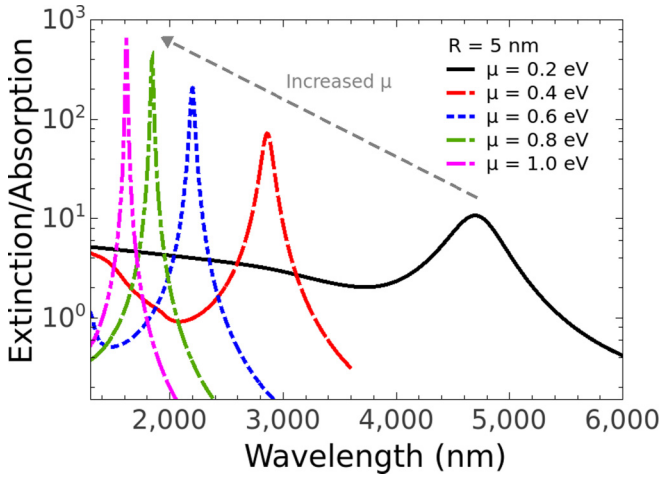

FIG. 3. Extinction/absorption spectrum of the graphene spherical shell, varying the excitation wavelength. We keep fixed the radius, $R = 5$ nm, of the graphene spherical shell for different values of chemical potentials, $\mu = 0.2$, 0.4, 0.6, 0.8, and 1.0 eV.

shell. In particular, the LSP resonance frequency is given as a solution of the equation [19]:

$$\frac{i\epsilon\omega_l}{2\pi\sigma(\omega_l)} = \left(1 + \frac{1}{2l+1}\right)\frac{l}{R}, \tag{1}$$

where R is the radius of the graphene spherical shell, ϵ is the dielectric permittivity of the surrounding medium and the space inside the graphene spherical shell and l is the resonance eigenvalue which is connected with the expansion order. Here we focus on graphene spherical shell radii where $R \ll \lambda$, where λ is the excitation wavelength, and thus we focus on the dipole mode $l = 1$. Since $R \ll \lambda$, the extinction and the absorption have essentially the same value (we disregard its scattering). Moreover, the LSP resonance depends on the intraband contributions of the surface conductivity, which, in the limit $\mu/\hbar\omega \gg 1$, $\sigma(\omega) = 4ia\mu/\hbar\omega$, ignoring the plasmon lifetime. Then the LSP resonance wavelength (λ_1) has the following value:

$$\lambda_1 = 2\pi c\sqrt{\frac{\hbar\varepsilon}{\pi a\mu}\frac{1}{12}R}. \tag{2}$$

In boundary element simulations, using MNPBEM [32], the graphene spherical shell is modeled as a thin layer of thickness $d = 0.5$ nm, with a dielectric permittivity [39],

$$\epsilon(\omega) = 1 + \frac{4\pi\sigma(\omega)}{\omega d}, \tag{3}$$

where the surface conductivity is given by Eq. (1) [9].

In Fig. 2, we present the absorption spectrum of the graphene spherical shell in the near-IR region, considering different values of its radius $R = 2.5$, 5, 10, and 15 nm. We consider a fixed value for the chemical potential, $\mu = 1$ eV, and observe that by increasing the radius of the graphene spherical shell the surface plasmon resonance is red-shifted as is predicted by Eq. (2). The dipole surface plasmon resonance from Fig. 2 for $R = 10$ nm is 2190 nm and from numerically solving Eq. (1) it is 2120 nm, validating our approach. Moreover, increasing the graphene spherical shell radius, the absorption strength gets higher.

In Fig. 3, we present the extinction spectrum of the graphene spherical shell, for fixed radius $R = 5$ nm, for different values of the chemical potential, $\mu = 0.2$, 0.4, 0.6, 0.8, and 1.0 eV. As the value of the chemical potential increases the graphene plasmon resonance is shifted to lower wavelengths as expected from Eq. (2). The physical explanation for such behavior is that the optical gap increases as the chemical potential value increases, and thus the surface plasmon resonance blue-shifts. For exploring the effect of coupling, we placed a QD (QE) inside graphene spherical shell. The optical properties of the QE are also described through its absorption spectrum. We here stress out that we do not take into account the emission of the QE itself. Response of a QD or QE can be safely modeled by a Lorentzian dielectric function [40,41].

$$\epsilon_{eg}(\omega) = \epsilon_\infty - f\frac{\omega_{eg}^2}{\omega^2 - \omega_{eg}^2 + i\gamma_{eg}\omega}, \tag{4}$$

where ϵ_∞ is the bulk dielectric permittivity at high frequencies, f is the oscillator strength [42,43], and γ_{eg} is the transition linewidth, which is connected to quality of the QE; ω_{eg} is connected with the energy from the excited to the ground state of the the QE. As the sphere is composed by a semiconducting material, it supports localized exciton polariton modes. The sphere sizes considered in this paper are much smaller than the excitation wavelength and only the dipole exciton resonance is excited. In the electrostatic limit, condition for exciting the dipole localized exciton resonance is given by the $\mathrm{Re}[\epsilon_{eg}(\omega)] = -2\epsilon$, where ϵ is the dielectric permittivity of the surrounding medium, where we consider $\epsilon = 1$. From this resonance condition it becomes apparent that changing the radius of the semiconducting sphere does not influence its resonance wavelength, as long as $R \ll \lambda$. On the other hand, as the level spacing of the QE changes, the position of the dipole localized exciton resonance shifts accordingly.

In Fig. 4, we consider the full case in which the QE is coated with a graphene spherical shell. We simulate the absorption of the combined system in the same spectral region. We start in Fig. 4 by considering the effect of the value of the chemical potential, μ, in the absorption of the combined system, where the value of the transition energy of the QE is fixed at $\lambda_{eg} = 1550$ nm. For the value of the chemical potential $\mu = 1$ eV, the splitting in the absorption spectrum is $\hbar\Omega = 84$ meV, where we can apparently see that the localized exciton mode is off-resonant to the surface plasmon mode. This means that the interaction between graphene plasmons and exciton modes is still in the strong-coupling regime. In addition, the initial splitting blue-shifts as the value of the chemical potential μ increases.

In Fig. 5, we present the absorption of the QE coated with a graphene spherical shell for $\mu = 1.2$ eV and the radius of the sphere is $R = 5$ nm. We consider different values of the transition energy of the QE, λ_{eg}. We observe that by increasing the value of λ_{eg}, the resonance of the exciton-polariton mode red-shifts; similarly, the splitting in the extinction/absorption of the combined QE core-graphene spherical shell nanosystem also red-shifts. For $\lambda_{eg} = 1400$ nm, where the

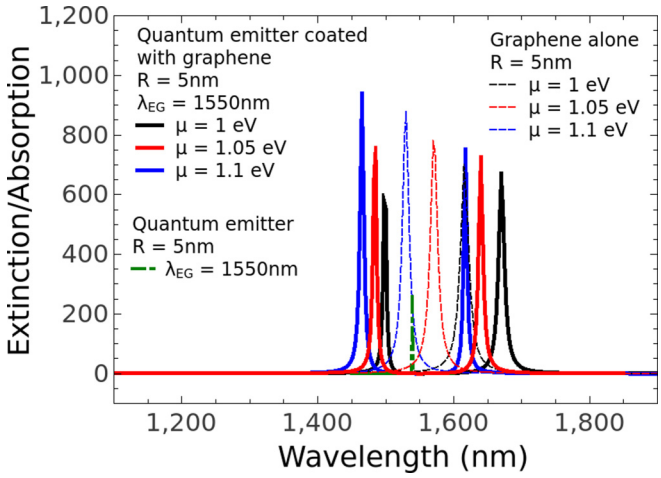

FIG. 4. Absorption spectra of the QE coated with the graphene spherical shell with respect to excitation wavelength. Different values of the chemical potential are employed while the QE transition energy is kept constant at $\lambda_{eg} = 1550$ nm. More details on simulation parameters are given in the inset.

exciton-polariton and the graphene plasmon modes are highly off-resonant, we still observe the plexitonic modes, which can also be read as the existence of the strong coupling between the nanostructures. In the following section, we explain this in more detail with a simple analytical model.

III. THE ANALYTICAL MODEL

Here we write the effective Hamiltonian for the graphene plasmons coupled to a QE and derive the equations of motion. We consider the QE as a two-level system [40] with level spacing $\omega_{eg} = 2\pi c/\lambda_{eg}$. In the steady state, we obtain a single equation. We show that by using this equation one can have a better understanding on the parameters of the combined system.

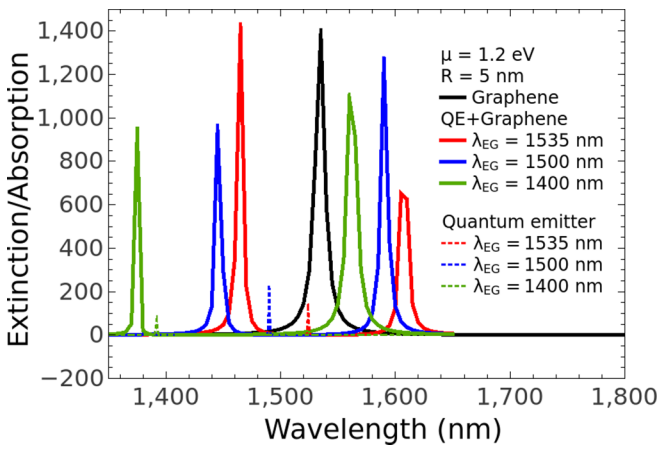

FIG. 5. Absorption spectra of the QE coated with the graphene spherical shell with respect to excitation wavelength. Fixed value for the chemical potential is taken as $\mu = 1.2$ eV, while different values of the transition energy of the QE are considered. More details in the inset.

We consider the dynamics of the total system as follows. The incident light (ε_L) with optical frequency $\omega = 2\pi c/\lambda$ excites graphene plasmons ($\hat{a}_{\rm GP}$), which are coupled to the quantum emitter. The Hamiltonian of the system can be written as the sum of the energy of the QE and graphene plasmon ($\omega_{\rm GP} = 2\pi c/\lambda_{\rm GP}$) oscillations ($\hat{H}_0$), the energy transferred by the pump source ($\hat{H}_L$)

$$\hat{H}_0 = \hbar\omega_{\rm GP}\hat{a}^\dagger_{\rm GP}\hat{a}_{\rm GP} + \hbar\omega_{eg}|e\rangle\langle e|, \tag{5}$$

$$\hat{H}_L = i\hbar(\varepsilon_L\hat{a}^\dagger_{\rm GP}e^{-i\omega t} - \text{H.c.}), \tag{6}$$

and the interaction of the QE with the graphene plasmon modes ($\hat{H}_{\rm int}$)

$$\hat{H}_{\rm int} = \hbar\{\Omega^*_R\hat{a}^\dagger_{\rm GP}|g\rangle\langle e| + \Omega_R|e\rangle\langle g|\hat{a}_{\rm GP}\}, \tag{7}$$

where the parameter Ω_R, in units of frequency, is the coupling strength between the graphene plasmon and the quantum emitter. $|g\rangle$ ($|e\rangle$) is the ground (excited) state of the QE. In the strong-coupling limit, one needs to consider counter-rotating terms in the interaction Hamiltonian [44], but there is still no analytically exact solution [45]. Instead of pursuing a full consideration, left for future work, we demonstrate here RWA, giving consistent results for the structure considered in this work. Moreover, we are interested in intensities but not in the correlations, so we replace the operators $\hat{a}_i$ and $\hat{\rho}_{ij} = |i\rangle\langle j|$ with complex numbers α_i and ρ_{ij} [46], respectively. The resulting equations of motion can be obtained as

$$\dot{\alpha}_{\rm GP} = -(i\omega_{\rm GP} + \gamma_{\rm GP})\alpha_{\rm GP} - i\Omega^*_R\rho_{ge} + \varepsilon_L e^{-i\omega t}, \tag{8a}$$

$$\dot{\rho}_{ge} = -(i\omega_{eg} + \gamma_{eg})\rho_{ge} + i\Omega_R\alpha_{\rm GP}(\rho_{ee} - \rho_{gg}), \tag{8b}$$

$$\dot{\rho}_{ee} = -\gamma_{ee}\rho_{ee} + i\{\Omega^*_R\alpha^*_{\rm GP}\rho_{ge} - \text{c.c.}\}, \tag{8c}$$

where $\gamma_{\rm GP}$ and γ_{eg} are the damping rates of the graphene plasmons and the off-diagonal density matrix elements of the QE, respectively. The values of the damping rates are considered as the same with previous section. The conservation of probability $\rho_{ee} + \rho_{gg} = 1$ with the diagonal decay rate of the QE $\gamma_{ee} = 2\gamma_{eg}$ accompanies Eqs. (8a)–(8c). In the steady state, one can define the amplitudes as

$$\alpha_{\rm GP}(t) = \tilde{\alpha}_{\rm GP}e^{-i\omega t}, \quad \rho_{ge}(t) = \tilde{\rho}_{ge}e^{-i\omega t}, \tag{9}$$

where $\tilde{\alpha}_{\rm GP}$ and $\tilde{\rho}_{ge}$ are constant in time. By inserting Eq. (9) into Eqs. (8a)–(8c), the steady-state solution of the graphene plasmons can be obtained as

$$\tilde{\alpha}_{\rm GP} = \frac{\varepsilon_L[i(\omega_{eg} - \omega) + \gamma_{eg}]}{(\omega - \Omega_+)(\omega - \Omega_-) + i\Gamma(\omega)}, \tag{10}$$

where $\Omega_\pm = \delta_+ \pm \sqrt{\delta^2_- - |\Omega_R|^2 y + \gamma_{eg}\gamma_{\rm GP}}$ defines hybrid mode resonances [47] and $\Gamma(\omega) = [\gamma_{eg}(\omega_{\rm GP} - \omega) + \gamma_{\rm GP}(\omega_{eg} - \omega)]$ with $\delta_\pm = (\omega_{\rm GP} \pm \omega_{eg})/2$ and population inversion $y = \rho_{ee} - \rho_{gg}$ terms.

It is important to note that the results presented in Figs. 6 and 7 are the exact solutions of Eqs. (8a)–(8c). We study the steady state in Eq. (10) to gain a better understanding of the parameters and avoid time-consuming electromagnetic 3D simulations of the combined system. Moreover, we hereafter calculate the intensity of the graphene plasmon mode in Eq. (8a), which is related to the absorption from the nanostructure [35].

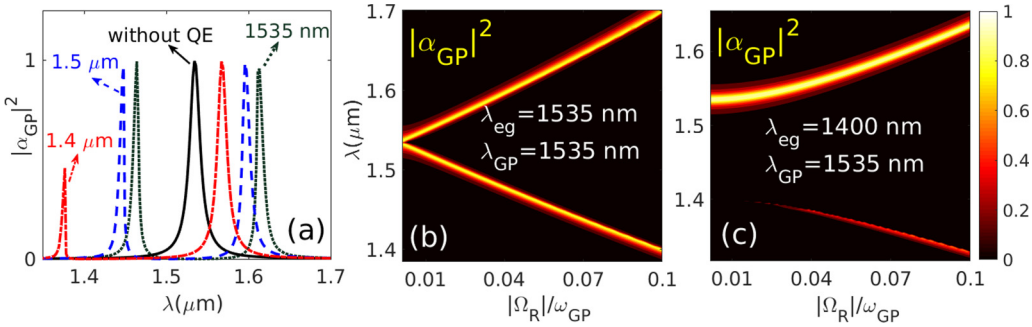

FIG. 6. The scaled absorption intensity of the graphene plasmon ($|\alpha_{GP}|^2$) as a function of excitation wavelength λ, obtained from Eq. (8a)–(8c). (a) In the absence (black solid) and in the presence of the QE having resonance at $\lambda_{eg} = 1535$ nm (dark gray dotted), $\lambda_{eg} = 1500$ nm (blue dashed), and $\lambda_{eg} = 1400$ nm (red dashed dotted) for a fixed coupling strength, $\Omega_R = 0.05\ \omega_{GP}$. Variation of the resonance intensity of graphene plasmon with excitation wavelength λ and coupling strength Ω_R for (b) $\lambda_{eg} = 1535$ nm and (c) $\lambda_{eg} = 1400$ nm. Here we use $\gamma_{GP} = 0.005\ \omega_{GP}$ and $\gamma_{eg} = 10^{-5}\ \omega_{GP}$.

To find the modulation of the intensities of the hybrid modes due to the presence of the quantum emitter, we use different resonance values: $\lambda_{eg} = 2\pi c/\omega_{eg} = 1535$, 1500, and 1400 nm in Fig. 6(a). The quantitative results comparing with the numerical simulations in Fig. 5, which takes retardation effects into account, are obtained. We also show the evolution of the hybrid modes by varying interaction strength $|\Omega_R|$ for zero detuning ($\delta_- = 0$) in Fig. 6(b) and for highly off-resonant case in Fig. 6(c). The strong-coupling regime is reached if the coupling strength exceeds the sum of the dephasing rates, e.g., $\Omega_R^2 > (\gamma_{GP}^2 + \gamma_{eg}^2)/2$ [48]. When the QE and the graphene plasmons become resonant [see Fig. 6(b)] a dip starts to appear around $|\Omega_R| \approx \gamma_{GP}$. This can be also read from Eq. (10). That is, when $\omega_{eg} = \omega_{GP} = \omega$, the Eq. (10) becomes $\tilde{\alpha}_{GP} \propto \gamma_{eg}/(|\Omega_R|^2 y + \gamma_{GP}\gamma_{eg})$. Since γ_{eg} is very small from other frequencies, with increasing $|\Omega_R|$, $\tilde{\alpha}_{GP}$ becomes smaller compared to case obtained without QE. Beyond a point, where the transparency window appears [40], there emerge two different peaks centered at frequencies $\Omega_\pm$, and the separation becomes larger as Ω_R increases.

This argument is not valid when the graphene plasmon and the level spacing of the QE are highly off-resonant. In this case, to make second peak significant, the interaction strength has to be much larger than γ_{GP} [see Fig. 6(c)]. The dip can be seen at ω_{eg}, which is out of the graphene plasmon resonance window and it may not be useful for practical applications. Having sharp peak due to strong coupling between off-resonant particles, however, can be very useful for the sensing applications. The reason for that it has smaller linewidth and can be tuned by changing chemical potential. To show this, in Fig. 7, we plot the evolution of the field intensity of the graphene plasmon ($|\alpha_{GP}|^2$) as a function of the excitation wavelength λ and the graphene plasmon resonance λ_{GP}, when graphene is alone Fig. 7(a) and with QE Fig. 7(b). It can be seen from Fig. 7(b) that it is possible to control the positions and linewidths of the hybrid resonances by adjusting μ. The similar behavior is also obtained in MNPBEM simulation (see Fig. 4).

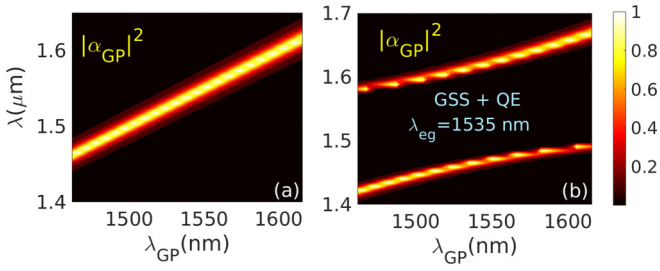

FIG. 7. The scaled field intensity of the graphene plasmon ($|\alpha_{GP}|^2$) as a function of excitation wavelength λ and graphene plasmon resonance λ_{GP}, when the graphene spherical shell is alone (a) and with QE (b). We scale graphene plasmon intensity with its maximum value and the parameters are used as $\Omega_R = 0.1\ \omega_{eg}$, $\gamma_{GP} = 0.01\ \omega_{eg}$, and $\gamma_{eg} = 10^{-5}\ \omega_{eg}$.

The several simplifications involved within the model, such as treating the emitter as a two-level system and considering only single plasmon mode, provided the quantitative results with 3D simulations. It was discussed in Ref. [49] that the quantitative results can also be obtained within this model by comparing its results with the experimental data in the strong-coupling regime, which also works well in the weak-coupling regime [50].

IV. SUMMARY

In summary, we investigate the optical response of the graphene plasmons for the spherical shell geometry in the presence and absence of the quantum emitter. We show that there is a tunability of the optical response of the graphene spherical shell through changing the value of the chemical potential and its radius. For the combined system (the QE covered with a graphene layer), we observe a splitting in the absorption band. This is due to the strong-coupling regime where splitting of up to 80 meV are observed in a single-QE limit. We also discuss the case when the QE and the graphene plasmons are off-resonant and observe that the system can hold strong coupling. The results of the theoretical model we present here support the solutions of the 3D Maxwell equations obtained from MNPBEM simulations.

Our results show that chemical potential and the coupling strength can be used as tuning parameters for tuning the extinction spectrum of the nanocomposite very effectively. Tuning of the chemical potential can be induced by the use

of an electrolytic cell [51] or by an electrical nanocontact through a scanning probe microscope tip, as shown in Fig. 1. The same tip can also be used to mechanically alter the graphene spherical shell-QE layout in a way to modify the coupling strength of the two counterparts through mechanical distortion of the graphene spherical shell. Having this tunability and the extreme spatial light confinement makes the graphene an important material in biosensor applications [52]. For instance, it can be used to selectively probe the protein at different frequencies [53] by tuning its plasmon resonance. And achieving such narrow linewidth plexcitonic modes can lead to even better sensitivity and spectral resolution in these applications. Additionally, having several parameters to play within this hybrid structure, such as radii of the spheres, the chemical potential, and the resonance frequency of the emitter, such a device can be fabricated in a more efficient way [54–57].

We expect our results to contribute to controlling light-matter interactions at the nanometer scale and find potential from all-optical switch nonlinear devices to sensing applications with current experimental ability for fabrication. Extreme field confinement, device tunability, and low losses make such structures even more attractive in future studies.

ACKNOWLEDGMENTS

This research was supported by The Scientific and Technological Research Council of Turkey (TUBITAK) Grant No. 117F118. M.E.T., A.B., and R.S. acknowledge support from TUBITAK 1001-119F101.

[1] A. K. Geim and K. S. Novoselov, The rise of graphene, in *Nanoscience and Technology: A Collection of Reviews from Nature Journals* (World Scientific, Singapore, 2010), pp. 11–19.

[2] J. Chen, M. Badioli, P. Alonso-González, S. Thongrattanasiri, F. Huth, J. Osmond, M. Spasenović, A. Centeno, A. Pesquera, P. Godignon *et al.*, Optical nano-imaging of gate-tunable graphene plasmons, Nature **487**, 77 (2012).

[3] Z. Fei, A. S. Rodin, G. O. Andreev, W. Bao, A. S. McLeod, M. Wagner, L. M. Zhang, Z. Zhao, M. Thiemens, G. Dominguez *et al.*, Gate-tuning of graphene plasmons revealed by infrared nano-imaging, Nature **487**, 82 (2012).

[4] Z. Fang, S. Thongrattanasiri, A. Schlather, Z. Liu, L. Ma, Y. Wang, P. M. Ajayan, P. Nordlander, N. J. Halas, and F. J. García de Abajo, Gated tunability and hybridization of localized plasmons in nanostructured graphene, ACS Nano **7**, 2388 (2013).

[5] M. Gullans, D. E. Chang, F. H. L. Koppens, F. J. G. de Abajo, and M. D. Lukin, Single-Photon Nonlinear Optics with Graphene Plasmons, Phys. Rev. Lett. **111**, 247401 (2013).

[6] F. J. García de Abajo, Graphene plasmonics: Challenges and opportunities, ACS Photon. **1**, 135 (2014).

[7] J. B. Khurgin and G. Sun, Impact of surface collisions on enhancement and quenching of the luminescence near the metal nanoparticles, Opt. Express **23**, 30739 (2015).

[8] L. Ju, B. Geng, J. Horng, C. Girit, M. Martin, Z. Hao, H. A. Bechtel, X. Liang, A. Zettl, Y. R. Shen *et al.*, Graphene plasmonics for tunable terahertz metamaterials, Nat. Nanotechnol. **6**, 630 (2011).

[9] K. S. Novoselov, Electric field effect in atomically thin carbon films, Science **306**, 666 (2004).

[10] A. N. Grigorenko, M. Polini, and K. S. Novoselov, Graphene plasmonics, Nat. Photon. **6**, 749 (2012).

[11] T. Low and P. Avouris, Graphene plasmonics for terahertz to mid-infrared applications, ACS Nano **8**, 1086 (2014).

[12] C. Liu, Z. Yu, D. Neff, A. Zhamu, and B. Z. Jang, Graphene-based supercapacitor with an ultrahigh energy density, Nano Lett. **10**, 4863 (2010).

[13] M. D. Stoller, S. Park, Y. Zhu, J. An, and R. S. Ruoff, Graphene-based ultracapacitors, Nano Lett. **8**, 3498 (2008).

[14] J.-S. Lee, S.-I. Kim, J.-C. Yoon, and J.-H. Jang, Chemical vapor deposition of mesoporous graphene nanoballs for supercapacitor, ACS Nano **7**, 6047 (2013).

[15] W.-C. Yen, Y.-Z. Chen, C.-H. Yeh, Jr-Hau He, Po-Wen Chiu, and Yu-Lun Chueh, Direct growth of self-crystallized graphene and graphite nanoballs with Ni vapor-assisted growth: From controllable growth to material characterization, Sci. Rep. **4**, 4739 (2014).

[16] H. Tan, J. Tang, J. Henzie, Y. Li, X. Xu, T. Chen, Z. Wang, J. Wang, Y. Ide, Y. Bando *et al.*, Assembly of hollow carbon nanospheres on graphene nanosheets and creation of iron–nitrogen-doped porous carbon for oxygen reduction, ACS Nano **12**, 5674 (2018).

[17] N. Daneshfar and Z. Noormohamadi, Optical surface second harmonic generation from plasmonic graphene-coated nanoshells: Influence of shape, size, dielectric core and embedding medium, Appl. Phys. A **126**, 55 (2019).

[18] H. J. Chandler, M. Stefanou, E. E. B. Campbell, and R. Schaub, Li@C_{60} as a multi-state molecular switch, Nat. Commun. **10**, 2283 (2019).

[19] T. Christensen, A.-P. Jauho, M. Wubs, and N. A. Mortensen, Localized plasmons in graphene-coated nanospheres, Phys. Rev. B **91**, 125414 (2015).

[20] T. Bian, R. Chang, and P. T. Leung, Optical interactions with a charged metallic nanoshell, J. Opt. Soc. Am. B **33**, 17 (2016).

[21] F. H. L. Koppens, D. E. Chang, and F. J. García de Abajo, Graphene plasmonics: A platform for strong light-matter interactions, Nano Lett. **11**, 3370 (2011).

[22] G. Toscano, S. Raza, W. Yan, C. Jeppesen, S. Xiao, M. Wubs, A.-P. Jauho, S. I. Bozhevolnyi, and N. A. Mortensen, Nonlocal response in plasmonic waveguiding with extreme light confinement, Nanophotonics **2**, 161 (2013).

[23] H.-S. Chu and C. How Gan, Active plasmonic switching at mid-infrared wavelengths with graphene ribbon arrays, Appl. Phys. Lett. **102**, 231107 (2013).

[24] Y. Li, H. Yan, D. B. Farmer, X. Meng, W. Zhu, R. M. Osgood, T. F. Heinz, and P. Avouris, Graphene plasmon enhanced vibrational sensing of surface-adsorbed layers, Nano Lett. **14**, 1573 (2014).

[25] O. Balci, N. Kakenov, E. Karademir, S. Balci, S. Cakmakyapan, E. O. Polat, H. Caglayan, E. Özbay, and C. Kocabas, Electrically switchable metadevices via graphene, Sci. Adv. **4**, eaao1749 (2018).

[26] L. Gaudreau, K. J. Tielrooij, G. E. D. K. Prawiroatmodjo, J. Osmond, F. J. G. de Abajo, and F. H. L. Koppens, Universal distance-scaling of nonradiative energy transfer to graphene, Nano Lett. **13**, 2030 (2013).

[27] K. J. Tielrooij, L. Orona, A. Ferrier, M. Badioli, G. Navickaite, S. Coop, S. Nanot, B. Kalinic, T. Cesca, L. Gaudreau, Q. Ma, A. Centeno, A. Pesquera, A. Zurutuza, H. de Riedmatten, P. Goldner, F. J. García de Abajo, P. Jarillo-Herrero, and F. H. L. Koppens, Electrical control of optical emitter relaxation pathways enabled by graphene, Nat. Phys. **11**, 281 (2015).

[28] J. A. Treadway, G. F. Strouse, R. R. Ruminski, and T. J. Meyer, Long-lived near-infrared MLCT emitters, Inorg. Chem. **40**, 4508 (2001).

[29] J. M. Pietryga, R. D. Schaller, D. Werder, M. H. Stewart, V. I. Klimov, and J. A. Hollingsworth, Pushing the band gap envelope: Mid-infrared emitting colloidal PbSe quantum dots. J. Am. Chem. Soc. **126**, 11752 (2004).

[30] S. Balci, O. Balci, N. Kakenov, F. B. Atar, and C. Kocabas, Dynamic tuning of plasmon resonance in the visible using graphene, Opt. Lett. **41**, 1241 (2016).

[31] S. J. Cartamil-Bueno, D. Davidovikj, A. Centeno, A. Zurutuza, H. S. J. van der Zant, P. G. Steeneken, and S. Houri, Graphene mechanical pixels for interferometric modulator displays, Nat. Commun. **9**, 4837 (2018).

[32] U. Hohenester and A. Trügler, Mnpbem—A matlab toolbox for the simulation of plasmonic nanoparticles, Comput. Phys. Commun. **183**, 370 (2012).

[33] D. G. Baranov, M. Wersäll, J. Cuadra, T. J. Antosiewicz, and T. Shegai, Novel nanostructures and materials for strong light-matter interactions, ACS Photon. **5**, 24 (2018).

[34] A. Manjavacas, F. J. García de Abajo, and P. Nordlander, Quantum plexcitonics: Strongly interacting plasmons and excitons, Nano Lett. **11**, 2318 (2011).

[35] L. Wu, H. Feng, M. Liu, K. Zhang, and J. Li, Graphene-based hollow spheres as efficient electrocatalysts for oxygen reduction, Nanoscale **5**, 10839 (2013).

[36] M. Jablan, H. Buljan, and M. Soljačić, Plasmonics in graphene at infrared frequencies, Phys. Rev. B **80**, 245435 (2009).

[37] L. A. Falkovsky, Optical properties of graphene, J. Phys.: Conf. Ser. **129**, 012004 (2008).

[38] B. Wunsch, T. Stauber, F. Sols, and F. Guinea, Dynamical polarization of graphene at finite doping, New J. Phys. **8**, 318 (2006).

[39] A. Vakil and N. Engheta, Transformation optics using graphene, Science **332**, 1291 (2011).

[40] X. Wu, S. K. Gray, and M. Pelton, Quantum-dot-induced transparency in a nanoscale plasmonic resonator, Opt. Express **18**, 23633 (2010).

[41] S. Postaci, B. C. Yildiz, A. Bek, and M. E. Tasgin, Silent enhancement of sers signal without increasing hot spot intensities, Nanophotonics **7**, 1687 (2018).

[42] R. Thomas, A. Thomas, S. Pullanchery, L. Joseph, S. M. Somasundaran, R. S. Swathi, S. K. Gray, and K. G. Thomas, Plexcitons: The role of oscillator strengths and spectral widths in determining strong coupling, ACS Nano **12**, 402 (2018).

[43] M. D. Leistikow, J. Johansen, A. J. Kettelarij, P. Lodahl, and W. L. Vos, Size-dependent oscillator strength and quantum efficiency of cdse quantum dots controlled via the local density of states, Phys. Rev. B **79**, 045301 (2009).

[44] M. O. Scully and M. S. Zubairy, *Quantum Optics* (Cambridge University Press, Cambridge, 1997).

[45] C. J. Gan and H. Zheng, Dynamics of a two-level system coupled to a quantum oscillator: Transformed rotating-wave approximation, Eur. Phys. J. D **59**, 473 (2010).

[46] M. Premaratne and M. I. Stockman, Theory and technology of SPASERs, Adv. Opt. Photon. **9**, 79 (2017).

[47] P. Vasa and C. Lienau, Strong light–matter interaction in quantum emitter/metal hybrid nanostructures, ACS Photon. **5**, 2 (2017).

[48] P. Törmä and W. L. Barnes, Strong coupling between surface plasmon polaritons and emitters: A review, Rep. Prog. Phys. **78**, 013901 (2015).

[49] M. Pelton, S. D. Storm, and H. Leng, Strong coupling of emitters to single plasmonic nanoparticles: Exciton-induced transparency and Rabi splitting, Nanoscale **11**, 14540 (2019).

[50] E. Kamenetskii, A. Sadreev, and A. Miroshnichenko, *Fano Resonances in Optics and Microwaves* (Springer, Berlin, 2018).

[51] See Supplemental Material at http://link.aps.org/supplemental/10.1103/PhysRevB.101.165412 for an alternative configuration for the proposed experimental setup.

[52] J. Peña-Bahamonde, H. N. Nguyen, S. K. Fanourakis, and D. F. Rodrigues, Recent advances in graphene-based biosensor technology with applications in life sciences, J. Nanobiotechnol. **16**, 75 (2018).

[53] D. Rodrigo, O. Limaj, D. Janner, D. Etezadi, F. J. G. De Abajo, V. Pruneri, and H. Altug, Mid-infrared plasmonic biosensing with graphene, Science **349**, 165 (2015).

[54] C. Valagiannopoulos, Maximal quantum scattering by homogeneous spherical inclusions, Phys. Rev. B **100**, 035308 (2019).

[55] D. C. Tzarouchis, P. Ylä-Oijala, and A. Sihvola, Unveiling the scattering behavior of small spheres, Phys. Rev. B **94**, 140301(R) (2016).

[56] A. Sihvola, D. C. Tzarouchis, P. Ylä-Oijala, H. Wallén, and B. Kong, Resonances in small scatterers with impedance boundary, Phys. Rev. B **98**, 235417 (2018).

[57] A. Sheverdin and C. Valagiannopoulos, Core-shell nanospheres under visible light: Optimal absorption, scattering, and cloaking, Phys. Rev. B **99**, 075305 (2019).